CrossMark

Analysis of future drought characteristics in China using the regional climate model CCLM

Jinlong Huang[1,4] · Jianqing Zhai[2,3] · Tong Jiang[2,3] · Yanjun Wang[2] · Xiucang Li[2,3] ·
Run Wang[5] · Ming Xiong[6] · Buda Su[1,2,3] · Thomas Fischer[3,7]

Abstract In this paper, the intensity, area and duration of future droughts in China are analyzed using the Standardized Precipitation Index (SPI) and the Standardized Precipitation Evapotranspiration Index (SPEI). The SPI and SPEI are used to evaluate the simulation ability of drought characteristics with the regional climate model COSMO-CLM (CCLM). The projected intensity and duration of future drought events are analyzed for the period 2016–2050 under three different respective concentration pathways (RCPs). The simulated and projected drought events are analyzed by applying the intensity-area-duration method. The results show that CCLM has a robust capability to simulate the average drought characteristics, while some regional disparities are not well captured, mainly the simulation of more drought events of shorter duration in Northwest China. For the future period 2016–2050, more intense dryness conditions are projected for China. An increase in evapotranspiration is found all over China, while a reduction in precipitation is apparent in the southern river basins. The increase in evapotranspiration plays an important role in the changes of future droughts over the northern river basins and southern river basins. Under RCP2.6, drought events of longer duration and with higher frequency are projected for the southwest and southeast of China. Under RCP4.5 and RCP8.5, a continuing tendency to more dry conditions is projected along a dryness band stretching from the southwest to the northeast of China. More frequent drought events of longer duration are projected in the southwestern river basins. For all future droughts, larger extents are projected, especially for events with long-term duration. The projected long-term drought events will occur more often and more severe than during the baseline period, and their central locations will likely shift towards Southeast China. The results of this study can be used to initiate and strengthen drought adaptation measures at regional and local scale, especially in the south of China.

Keywords Drought · Intensity · Area · Duration · CCLM · China

✉ Buda Su
subd@cma.gov.cn

✉ Thomas Fischer
thomas.fischer.geo@gmx.de

[1] State Key Laboratory of Desert and Oasis Ecology, Xinjiang Institute of Ecology and Geography, Chinese Academy of Sciences, Urumqi 830011, China

[2] Collaborative Innovation Center on Forecast and Evaluation of Meteorological Disasters/School of Remote Sensing, Nanjing University of Science and Technology, Nanjing 210044, China

[3] National Climate Center, China Meteorological Administration, Beijing 100081, China

[4] University of Chinese Academy of Sciences, Beijing 100049, China

[5] Faculty of Resources and Environment, Hubei University, Wuhan, China

[6] Bureau of Hydrology, Changjiang Water Resources Commission, Wuhan, China

[7] Department of Geosciences, Eberhard Karls University, Tübingen, Germany

1 Introduction

Since the late twentieth century, a trend to warmer average temperatures is observed for most parts of the World (Hansen et al. 2010; Rohde et al. 2013). A continuation of this trend is projected by many climate models under most emission scenarios and concentration pathways, which

calculate an increase in the surface temperature of about 0.7–2.4 °C by the year 2050 relative to the reference period 1986–2005 (Collins et al. 2013). Field et al. (2012) presume that due to the increase in global temperatures, unprecedented intense climate events (e.g. floods and droughts) might occur. Although the observed trend in global drought events varies over temporal and spatial scales (Park et al. 2015), more severe droughts occurred in the early twenty-first century, e.g. the 2010 drought in Australia (Cai et al. 2014), the 2011–2012 drought in the United States (Seneviratne 2012), and the 2011 drought in southern China (Sun and Yang 2012). Drought is a space–time dimension process of insufficient water availability usually characterized by its intensity, spatial extent, and duration (Xu et al. 2015; Sheffield and Wood 2007). There are three main types of droughts depending on the system (climate, agriculture, and hydrology) in focus, i.e. meteorological drought (e.g. Duffy et al. 2015), agricultural drought (e.g. Wang et al. 2005), and hydrological drought (e.g. Wong et al. 2013). In general, droughts predominantly result from decreases in precipitation amounts and increased evaporation, which might be related to a warming climate, and have profound impacts on ecosystems and the society (Vicente-Serrano et al. 2012; Dai 2013). Information on potential changes in future drought characteristics are needed for managing local drought risks, mitigating possible impacts on numerous socio-economic sectors, and developing adaptation strategies (Hirabayashi et al. 2008; Svoboda et al. 2015).

Climate models are regarded as a key tool to provide possible tendencies in future climate variables based on different emission scenarios (i.e. SRES) or concentration pathways (RCPs). The confidence in projecting such future climate variables is related to the ability of a climate model in reproducing the past and present climate patterns and their trends (Raisanen 2007; Reifen and Toumi 2009; McMahon et al. 2015). The Coupled Model Intercomparison Project phase 5 (CMIP5) organized by the World Climate Research Program (WCRP) has provided multi-model simulations (Meehl et al. 2000, 2007; Taylor et al. 2012), which contributed to the Fifth Assessment Report of the Intergovernmental Panel on Climate Change (IPCC AR5) and several other climate change assessment reports. Although consistent tendencies with the observations are reproduced by the CMIP5 model ensembles at a global scale, the regional dryness and wetness tendencies are hardly captured, while the drought area identified by the drought index is overestimated by most CMIP5 models (Nasrollahi et al. 2014). At regional scales, global climate models (GCMs) often induce rather large errors due to their poor representation of the regional atmospheric processes and climatic feedbacks. Therefore, adequate spatial resolution is needed to resolve the physical processes by regional climate models (RCMs) (Gao et al. 2006; Yu et al. 2010). The improvements in

RCMs, especially their ability in reproducing the regional values and patterns in precipitation, temperature, and evaporation, allows more realistic climate impact assessments providing more accurate and credible information on potential impacts of climate extremes, e.g. droughts (Liang et al. 2004, 2008). Therefore, a RCM dynamically downscaled from a CMIP5 model (i.e. MPI-ESM-LR) will be used in the current study.

Based on datasets of GCMs, many scientists have conducted research on projected future drought characteristics (Orlowsky and Seneviratne 2013; Park et al. 2015; Zarch et al. 2015). One major finding sees the drought risk increasing at global scale during the whole twenty-first century (Sheffield and Wood 2008; Dai 2013). Regional projections of drought characteristics for different continents and regions of high vulnerability are necessary for developing adaptation strategies and disaster response measures (Sheffield et al. 2009). For example, Burke and Brown (2007) assessed the drought risk in southern Africa and forecast an increasing risk due to the modeled decrease in annual average precipitation. For North America, the changes in the frequency and severity of droughts have been projected by Wehner et al. (2011). In contrast, a lesser frequency, weaker intensities, and shorter durations in drought are projected for entire Asia. But strong increases in the standard deviation of mean precipitation for the monsoon regions of Asia and decreasing precipitation in West Asia are projected to result in an increase in drought frequency and intensity in these regions (Kim and Byun 2009; Dai 2013).

Based on past drought events, China is prone to costly drought impacts, e.g. with an average annual drought-affected crop area of 209,000 km^2 and annual direct economic losses of more than 32 billion Yuan (according to 2013 price levels) in the period from 1949 to 2013 (Zhai et al. 2014; Qin et al. 2015). Previous studies on observation data found significant trends towards dryness mainly in a regional band from the southwest to the northeast of China, while significant trends toward wet conditions were mainly observed in the northwestern parts of China (Shi et al. 2003; Zhai et al. 2010a, b; Qian et al. 2011; Zhao et al. 2012; Tao et al. 2014). In areas of this regional dryness band, drought events occurred more frequently and more severe in the most recent decades (Fischer et al. 2011; Yang et al. 2012; Zhang et al. 2013; Yu et al. 2014a, b). Additionally, Zhai et al. (2016) analyzed the intensity, contiguous area, and duration (IAD) of past drought events in China by applying an IAD analysis method. Their results allow comprehensive statements on the severity of historical drought events. Furthermore, a continuing tendency to more intense dry conditions is projected for the observed dryness band based on findings of a GCM with a SRES A2 scenario (Zhai et al. 2010a, b). Under the A1B scenario,

drought will increase in southern Tibet, Southwest China, the middle and lower Yangtze River basin, and Northeast China (Liu et al. 2012). Using the CMIP5 models under the newer RCPs, higher drought risks are projected in Southwest and East China for the twenty-first century (Wang and Chen 2014; Yin et al. 2015).

Currently, studies on future drought characteristics in China mainly use GCMs under RCPs or RCMs under SRES. For regional drought analyses, it seems necessary to apply state-of-the-art RCMs under RCPs to further increase the knowledge of potential drought impacts in China. Additionally, most of the existing studies on drought mainly focus on station- or grid-based projections of climate variables and only using one-dimensional methods without considering the spatial extent of drought events (Biondi et al. 2008). In order to better understand the future drought characteristics, in this study, the regional climate model Cosmo-CLM (CCLM) is evaluated on observations for the baseline period 1961–2005, and future changes in drought events for China are projected by using the CCLM under different RCPs. The modeled climate variables are used to calculate the SPI and SPEI. The results are analyzed in a space–time dimension by applying the Intensity-Area-Duration method (Zhai et al. 2016) to obtain information on potential drought intensities and contiguous drought-affected areas at predefined durations for the period 2016–2050.

2 Data and methods

2.1 Observational data

Quality-proven monthly precipitation, temperature (mean, maximum, minimum), air pressure, relative humidity, wind speed, and sunshine duration from 530 meteorological stations in China for the period 1961–2005 as provided by the National Meteorological Information Center of the China Meteorological Administration were used in this study (Fig. 1).

2.2 Simulation data

The regional climate model CCLM has been developed out of the weather forecast model 'Lokal Modell' (Rockel et al. 2008), which was developed by the German Weather Service (DWD). The atmospheric circulation is described on the basis of primitive thermo-hydro-dynamical equations at resolutions between 1 and 50 km. Climate simulations with a high spatial resolution of about 50 km are carried out with CCLM in the CORDEX-East-Asia domain (http://www.cordex.org) (Giorgi et al. 2009). CCLM, based on downscaled GCMs under different SRES scenarios, has

already been applied in various studies on changing climate variables (e.g. precipitation, temperature) in China (Fischer et al. 2013; Cao et al. 2013; Wang et al. 2013).

In this study, the latest GCM from the Max Planck Institute, the Earth System Model running on a low resolution grid (MPI-ESM-LR) serves as the data input for global climate change projections (Giorgetta et al. 2013). The MPI-ESM is a comprehensive Earth System Model consisting of general circulation models for the atmosphere (ECHAM6), the land surface (JSBACH), and the ocean and sea ice (MPIOM). A nesting approach is used in CCLM to downscale the GCM with a coarse resolution. CCLM runs with a spatial resolution of 0.44° (50 km) on a rotated coordinate system. For analytical purpose, CCLM is interpolated into a regular geographical grid with a 0.5° × 0.5° resolution by applying the bilinear interpolation method. The CCLM-simulated datasets of precipitation, temperature (mean, maximum, minimum), air pressure, relative humidity, wind speed and sunshine duration for China are evaluated for the years 1961–2005, while projected future changes in drought characteristics under three RCPs (RCP2.6, RCP4.5, and RCP8.5) are analyzed for the years 2016–2050. The RCP2.6, RCP4.5, and RCP8.5 represent a low concentration, a stable concentration, and a high concentration of emissions, respectively (van Vuuren et al. 2011). To obtain the future changes in wind field at 850 hPa relative to the baseline period 1961–2005, the simulated atmospheric circulation pattern are reproduced by MPI-ESM-LR with a resolution of 1.875° × 1.875° for the period 1961–2005 and 2016–2050, respectively. The spatial distribution of the CCLM grid over the ten major hydrological regions of China is shown in Fig. 1.

2.3 Drought indices

There are three main types of droughts depending on the system (climate, agriculture, and hydrology) in focus, i.e. meteorological drought (e.g. Duffy et al. 2015), agricultural drought (e.g. Wang 2005), and hydrological drought (e.g. Wong et al. 2013). These types can be represented by multi-scale drought indices. Our research focusses on the hydrological drought in China. In our study, the well-known multi-scale standardized precipitation index (SPI) and the standardized precipitation-evapotranspiration index (SPEI) are used (McKee et al. 1993; Vicente-Serrano et al. 2010). The 1- to 3-months SPI/SPEI is usually used to reflect the status of soil moisture. The changes in soil moisture in the lower layers as well as in river runoff are better reflected with a 6- to 24-months SPI/SPEI (WMO 2012). Similar as the research by Zhai et al. (2010a, b, 2016), we focus on the hydrological drought, which is assumed to be best reflected with the 12-months SPI/SPEI, as with a time scale of 12 months the highest correlation coefficients between
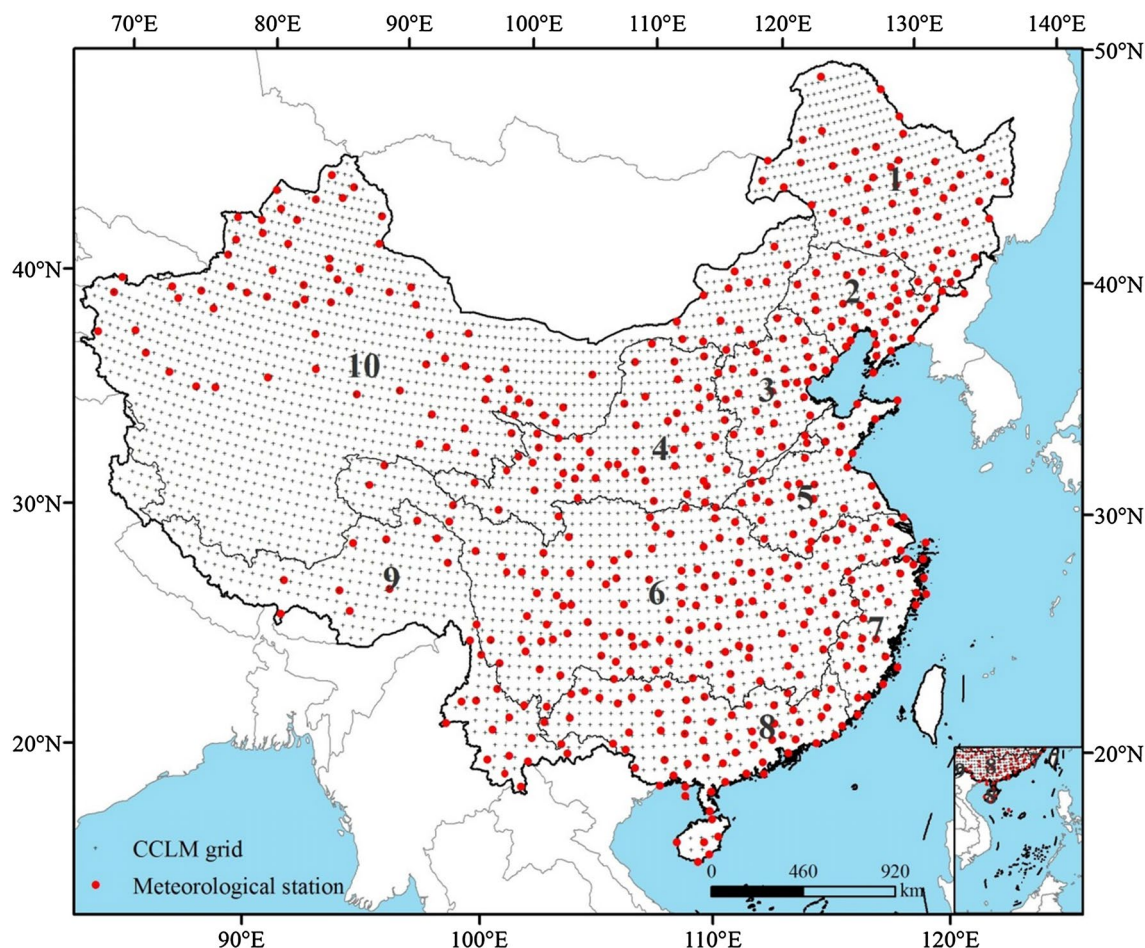
Fig. 1 The spatial distribution of meteorological stations and the CCLM grid over the ten major hydrological regions of China (*1* Songhuajiang River basin, *2* Liaohe River basin, *3* Haihe River basin, *4* Yellow River basin, *5* Huaihe River basin, *6* Yangtze River basin, *7* Southeast river basins, *8* Zhujiang River basin, *9* Southwest river basins, *10* Northwest river basins)

SPI and runoff anomaly are found in numerous river basins of China. Both multi-scale indices are used to analyze the characteristics of future hydrological droughts in China.

A detailed description of the design of the SPI can be found in McKee et al. (1993) and Wu et al. (2005). For the SPI, the shape parameter and scale parameter of precipitation are estimated based on the fitted Gamma distribution (Bordi and Sutera 2002). Following this, the SPI is calculated by transforming the fitted distribution to a normal distribution. By using the estimated parameters for the baseline period (1961–2005), the cumulative probability of future SPI values (2016–2050) can be compared and then transformed to a normal variable.

Future changes in aridity or drought should also consider the climate variables such as temperature, wind, water vapor pressure etc. (PaiMazumder and Done 2014). The SPEI proposed by Vicente-Serrano et al. (2010) is suitable for the impacts of global warming on drought, as it considers the potential evapotranspiration. The SPEI is designed to quantify the difference between monthly mean precipitation and potential evapotranspiration (PET) at multiple timescales reflecting the impacts of droughts on different water resources (Tao et al. 2014; Begueria et al. 2014). For the *i*-month timescale, a window length of *i* months is used to accumulate the difference between the monthly mean precipitation and PET. This preprocessing is calculated as follows:

$$D_{k+i-1} = \sum_{k=1}^{n-i+1} P_k - PET_k$$

where, i is the time scale, P_k and PET_k denote the monthly precipitation and potential evapotranspiration at k time, respectively, and n is the length of the data record of the station.

The PET is calculated by the Penman–Monteith equation as recommended by the Food and Agriculture Organization (FAO) (Allen et al. 1998). The difference between

precipitation and evapotranspiration is fitted to the Log-logic distribution and transformed to a normal distribution (Vicente-Serrano et al. 2010). The distribution function parameters estimated in the period 1961–2005 is used for the calculation of the future SPEI, which means the dryness or wetness conditions in future can be compared to the baseline period.

While $-1 < \text{SPI(SPEI)} \leq 0$ denote dry conditions near normal, a SPI(SPEI) ≤ -1, -1.5, -2 denote a moderate, severe, and extreme drought, respectively. In this paper, the contributions of precipitation and evapotranspiration to droughts are analyzed by the comparison of SPI and SPEI.

2.4 Trend analysis

For detecting the trends and tendencies in the SPI/SPEI time-series as well as testing the significance of variation, the widely used non-parametric Mann–Kendall (MK) test is applied (Gemmer et al. 2008; Zhai et al. 2016). The value of the MK statistic (*MKs*) denotes the tendency and its significance. Here a *MKs* >1.96 means a significant positive trend and a *MKs* <−1.96 denotes a significant negative trend, both at the 95% confidence level.

2.5 RCM evaluation

The spatial patterns of CCLM-simulation are evaluated by the spatial correlation coefficient (SCC) between the MK statistics of the observation and of the simulation. The SCC is defined as:

$$SCC = \frac{\sum_{i=1}^{t}(CCLM_i - \overline{CCLM_i})(Obs_i - \overline{Obs_i})}{\sqrt{\sum_{i=1}^{t}(CCLM_i - \overline{CCLM_i})^2 \sum_{i=1}^{t}(Obs_i - \overline{Obs_i})^2}}$$

where, $CCLM_i$ (OBS_i) is the MK-value of the CCLM-simulation (observation) at station i, $\overline{CCLM_i}(\overline{Obs_i})$ denote the mean of all the grid points in the CCLM-simulation (observation), t denotes the total number of station points in the spatial field (Gao et al. 2012a). The significance of the correlation coefficient is tested by the p value which is computed using a Student's t distribution for a transformation of the correlation. The correlation is significant if $p \leq 0.05$.

2.6 Intensity-area-duration analysis

In general, drought is a space–time dimension process usually characterized by its intensity, spatial extent, and duration (Xu et al. 2015; Sheffield and Wood 2007). Traditionally, the drought intensity and duration are extracted from the time series of a drought index for a certain grid point, while the drought area is obtained only by the accumulation of such grid points. In this study, the intensity, contiguous area, and duration of droughts are identified at temporal

and spatial scale by using a cluster analysis method, the Intensity-Area-Duration (IAD) method, as described in Andreadis et al. (2005) and Sheffield et al. (2009). This method has been already applied for China by Zhai et al. (2016). The IAD method spatially connects similar regions (or cluster) with drought conditions, i.e. a SPI/SPEI ≤ -1. Based on this, separate drought clusters (drought events) with different area sizes are identified in the follow-up. For each drought event, the cluster algorithm starts at the drought center (lowest SPI/SPEI value) and attaches the adjacent grid with a low SPI/SPEI value. When all grids with a SPI/SPEI ≤ -1 are incorporated in the drought event, the contiguous area (accumulation) and the intensity (average) are calculated and listed in the database. More details and descriptions on this cluster analysis method can be derived from Zhai et al. (2016). Based on the results, the IAD curves are constructed for each drought event with a predefined duration (e.g. 1, 3, 6, 9, 12, 24 months). The IAD envelope curve, extracted from the IAD curves, shows the time and intensity per contiguous drought area and for a specific duration.

3 Results

3.1 Evaluation of CCLM simulations

As the SPI and SPEI are both standardizations of precipitation or the difference between precipitation and potential evapotranspiration, the simulation ability of CCLM relates to the ability in reproducing the precipitation and potential evapotranspiration. Spatial patterns of the observed and simulated average annual precipitation and potential evapotranspiration are presented in Fig. 2. The SCC of precipitation between the observation and the CCLM-simulation is 0.71, which is significant at the 99% confidence level. The Songhuajiang, Liaohe, and Huaihe River basins are all well simulated with coefficients of 0.80, 0.89, and 0.87, respectively (Table 1). However, CCLM simulates higher precipitation in Southwest China and the Tibetan Plateau, while less precipitation is simulated in Southeast China. Compared to the observed data, the precipitation in North China is less biased.

The SCC of the potential evapotranspiration between the observation and the CCLM-simulation is 0.53, which is significant at the 99% confidence level. The potential evapotranspiration in the northeastern river basins is also well simulated and less biased. The SCCs of the Songhuajiang, Liaohe, and Yellow River basins are 0.94, 0.80, and 0.90, respectively (Table 1). All ten large river basins are passing the test of significance at the 95% confidence level. The overestimation of potential evapotranspiration is mainly located in the Huaihe, Zhujiang, and lower Yangtze
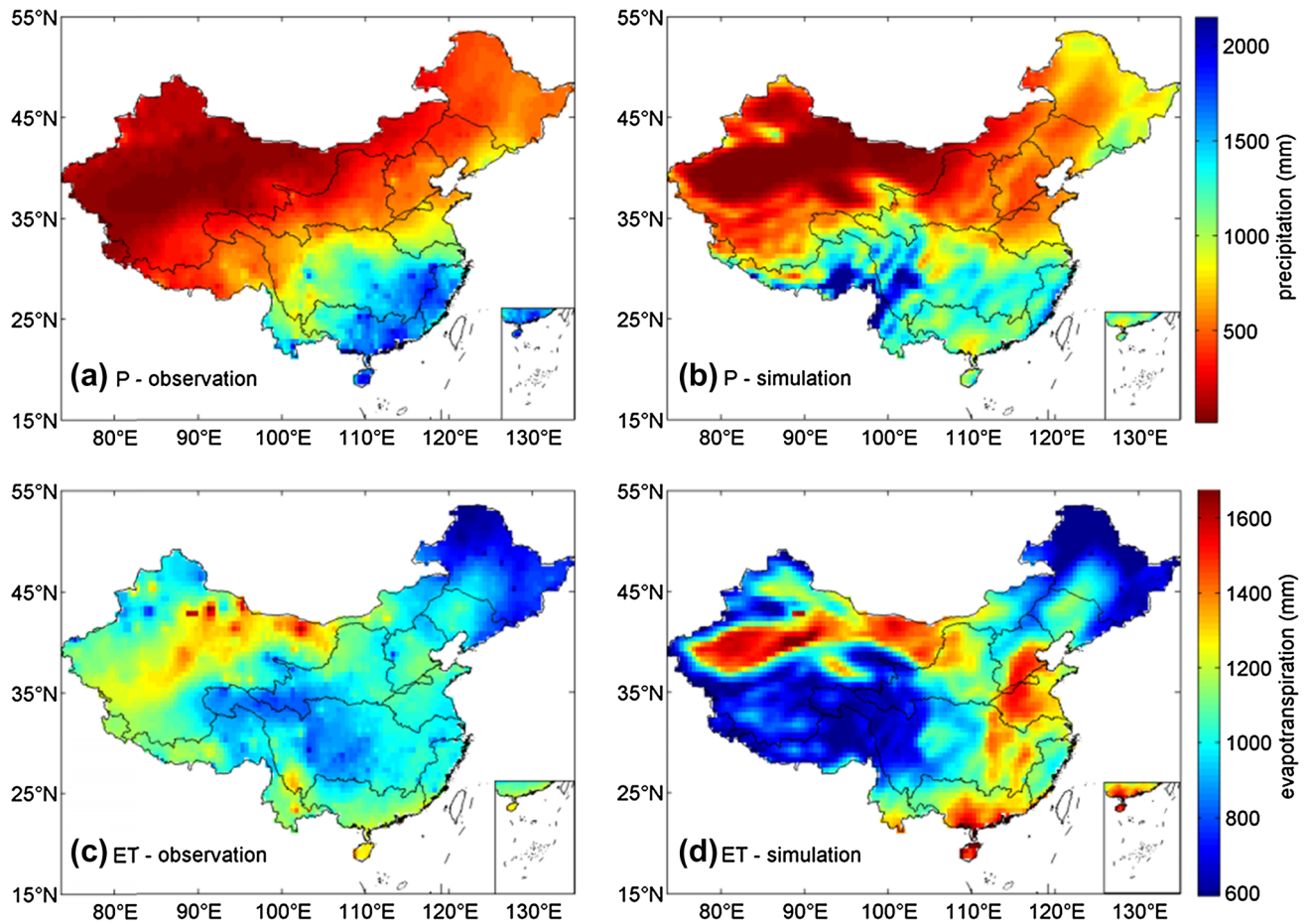
Fig. 2 Spatial distribution of the observed and simulated average annual precipitation (**a, b**) and potential evapotranspiration (**c, d**) in China for the period 1961–2005

Table 1 Spatial correlation coefficients and biases of precipitation and evapotranspiration between observation and CCLM-simulation of the major river basins in China during 1961–2005

Regions	Precipitation		Evapotranspiration	
	SCC	Bias (mm)	SCC	Bias (mm)
Songhuajiang	0.80[a]	250	0.94[a]	−78
Liaohe	0.89[a]	112	0.80[a]	23
Haihe	−0.29[a]	8	0.75[a]	148
Yellow	0.55[a]	144	0.90[a]	41
Huaihe	0.87[a]	−177	0.20	319
Yangtze	0.25[a]	135	0.33[a]	19
Southeast	−0.07	−234	0.69[a]	92
Zhujiang	−0.05	−388	0.78[a]	191
Southwest	0.36[a]	744	0.46[a]	−271
Northwest	0.73[a]	147	0.44[a]	−112

[a] Significant at 99% confidence level

River basins, while an underestimation occurs in Southwest China and the Tibetan Plateau of higher elevation.

To evaluate the ability of CCLM in reproducing the drought characteristics in China, the overall distribution characteristics and spatial patterns of the number and average duration of observed and simulated drought events (SPI/SPEI $\leq −1$) in China are shown in Fig. 3. For this purpose, drought number and duration are extracted from the drought events without considering the contiguous drought area. The number of droughts is counted and the duration of droughts is calculated by averaging all events' duration at each grid. CCLM simulates the overall distribution characteristics of the observed drought number well with 15–20 droughts in most grids. During the period 1961–2005, most droughts (more than 21 events per grid) have been observed mainly in the southern and eastern parts of China (Fig. 3b, d). Based on the classification into five groups of drought numbers, the simulated number of events identified by SPI/SPEI fit the observations at around 37% (31%) of all grids. The CCLM-simulated events identified by SPI show a lower frequency in the south, but a higher frequency in
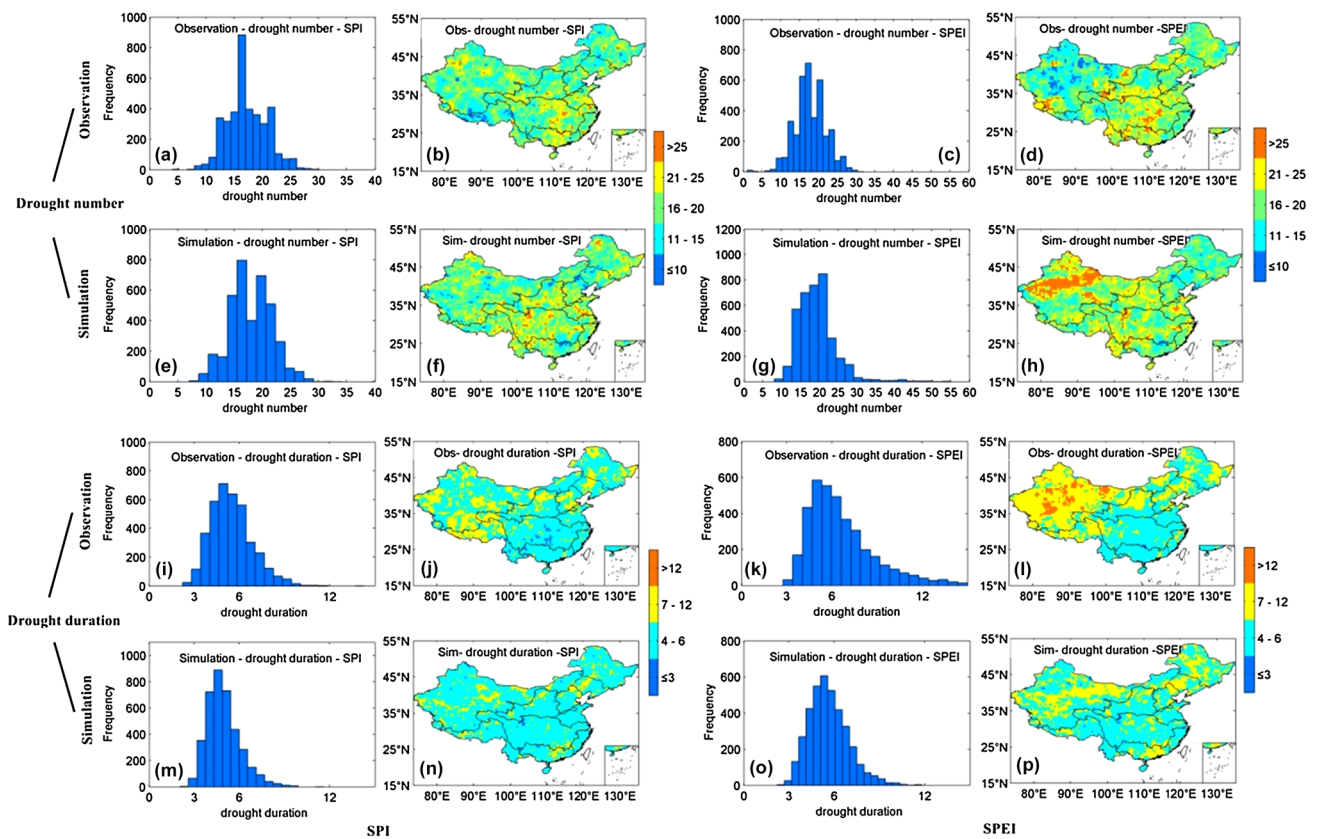
Fig. 3 Overall distribution characteristics of observed and simulated number and duration of drought events and their spatial distributions based on the SPI and SPEI of China for the period 1961–2005

the central and southwestern parts of China (Fig. 3f). An overestimation in the number of drought events obtained from the SPEI is found in Northwest China.

During 1961–2005 droughts with duration of 4–6 months are most common, which are well captured by CCLM using both SPI and SPEI (Fig. 3). For droughts identified by the SPI, short-to-medium-term events (4–6 months) are mainly simulated in the south and east of China, while medium-term events (7–12 months) are mainly located in parts of the northwestern and northeastern river basins. The simulated duration of drought events fit the observations at around 63% of all grids. For SPEI droughts, short-to-medium-term events are also mainly simulated in the south and east of China, especially in the Zhujiang River basin and the middle and lower Yangtze River basin (Fig. 3l). Droughts with longer duration are found in the northwestern river basins and parts of the Yellow, Haihe, Liaohe, and Songhuajiang River basins. Compared to the observations, about 53% of the grid points show similar average durations, while shorter durations are simulated by CCLM for the northwestern river basins but longer durations in the eastern Zhujiang River basin (Fig. 3p).

3.2 Projected changes in SPI and SPEI

Droughts are influenced by the decrease in precipitation and the increase in evapotranspiration. Changes of precipitation and evapotranspiration in 2016–2005 relative to 1961–2005 are presented in Fig. 4. Under RCP2.6, large decreases in precipitation are shown in the southwest and southeast of China, while large increases are projected in the northeast river basins. Under RCP4.5 and RCP8.5, the decreases are mainly located in the southwestern to northeastern regions of China. For evapotranspiration, increases are found all over China with relative large changes projected in the Huaihe River basin under both RCP2.6 and RCP4.5, and in the northeast river basins under RCP8.5.

By applying the same distribution function parameters estimated for the baseline period 1961–2005 to the future SPI/SPEI, the dryness/wetness conditions relative to the 1961–2005 can be compared. Each box in Fig. 5 is constructed based on the 45 years' (1961–2005) or 35 years' (2016–2050) dryness/wetness conditions. The changes in observed and projected SPI/SPEI are calculated under three RCPs relative to the baseline period (Fig. 4). SPI(SPEI) <0 indicates dryness, while SPI(SPEI) >0 denotes wetness.
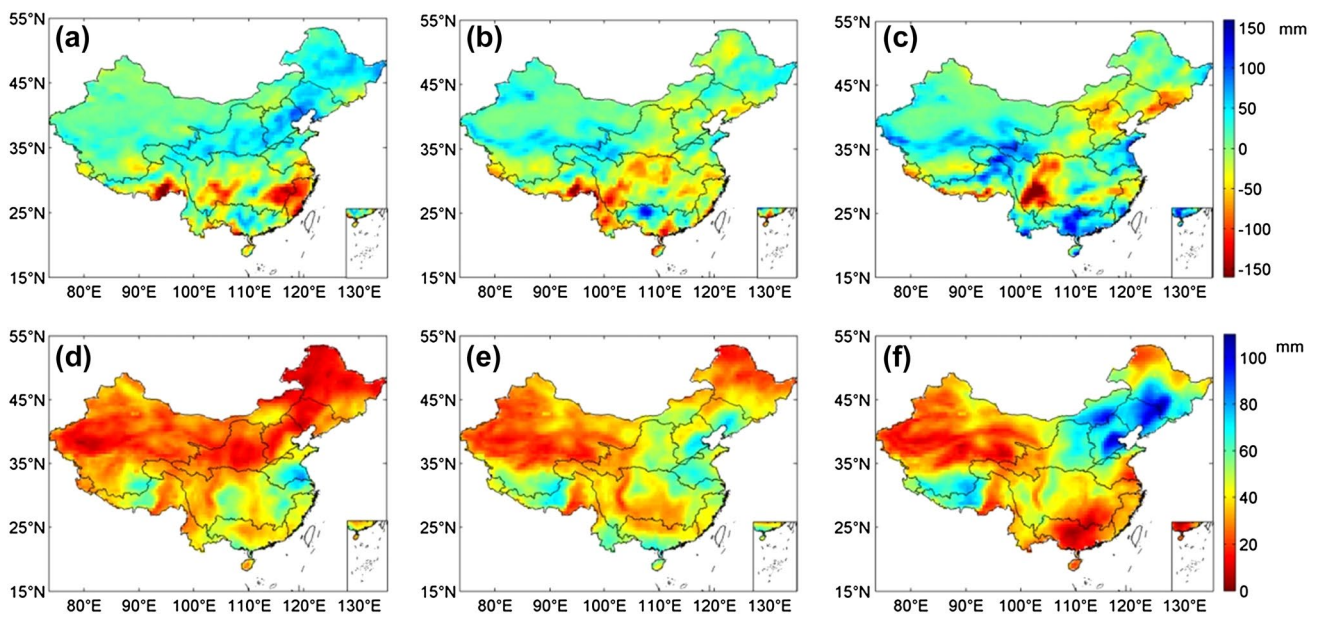
Fig. 4 Projected changes in spatial patterns in precipitation (**a–c**) and evapotranspiration (**d–f**) under RCP2.6 (**a, d**), RCP4.5 (**b, e**) and RCP8.5 (**c, f**) over China for the period 2016–2050 relative to 1961–2005
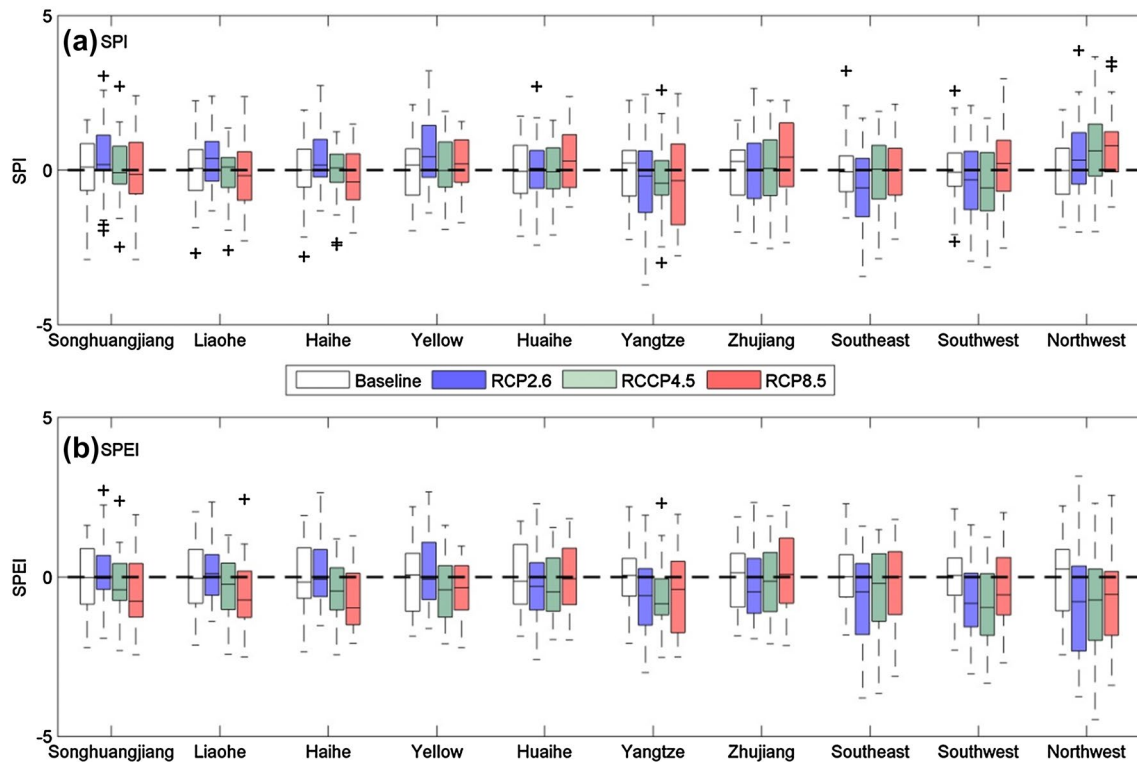

Fig. 5 Changes in drought indexes SPI (**a**) and SPEI (**b**) under three different RCPs over ten large river basins of China for the period 2016–2050; *boxes* show the interquartile range, *horizontal lines* the median, and the whiskers extent to the minimum/maximum value within the 1.5 interquartile range of the lower/upper quartile; The crosses represent the outliers outside the 1.5 interquartile range of the lower/upper quartile

For the changes in SPI (Fig. 5a), relative to 1961–2005, most years in future are projected to become wetter in Songhuajiang River basin, Liaohe River basin, Haihe River basin, Yellow River basin and Northwest river basins, while a dryness tendency is found in the Yangtze River basin and the Southeast and Southwest river basins under RCP2.6. Under RCP4.5, strong dryness trends are found in the Yangtze River basin and the Southwest river basins, but a wetness tendency in the Northwest river basins. The Yangtze and the Northwest river basins also get drier and wetter under RCP8.5, respectively. But a dryness tendency is found in the Songhuajiang, Liaohe, and Haihe River basins, and a wetness tendency in the Southwest river basins in most of the years under RCP8.5, which is contrary to the RCP2.6.

In contrast to the changes in SPI, the changes in SPEI (Fig. 5b) show more severe dryness conditions in the northern river basins, namely the Songhuajiang, Liaohe, Haihe, Yellow, and Huaihe River basins. Similar changes are found in the Yangtze, Southeast and Southwest river basins, while a contrasting dryness change under all RCPs is found in the Northwest river basins relative to the baseline period. From low to high emission pathways, the northern river basins are more likely to become drier, while the southern river basins are projected to become wetter.

The spatial patterns of projected changes in the CCLM-simulated SPI/SPEI are calculated for the three RCPs over China for the period 2016–2050 relative to 1961–2005 (Fig. 6). For the change in SPI under RCP2.6 (Fig. 6a),

multiple grids with statistically significant changes towards wet conditions are found in the Songhuajiang River basin (85% of all grids in the river basin), the Liaohe River basin (84%), Haihe River basin (87%), the north of Huaihe River basin (36%), Yellow River basin (88%), and the Northwest river basins (65%). Significant changes towards dry conditions are mainly shown in the Yangtze River basin (36%), and Southeast river basins (93%). In the low emission RCP, the regions with projected increases in dry conditions are moving towards the south of China, indicating that more drought impacts can be expected in South China, but less in the central north. Under RCP4.5 (Fig. 6b), significant changes towards dry conditions are mainly shown in the west of Songhuajiang River basin (15%), east of Liaohe River basin (27%), Yangtze River basin (50%), the Southwest river basins (68%). The significant negative changes are mainly located in the observed dryness band. The spatial patterns of significant changes toward dry conditions under RCP8.5 are similar to RCP4.5, as significant trends toward dryness conditions are simulated in the regions from the southwest to the northeast of China (Fig. 6c).

Under all RCPs, similar changes in the SPI are located in Southwest China with changes toward dry conditions. For the dryness or wetness changes detected by SPEI, dryness changes are found almost all around China, except for parts of the northeastern river basins under RCP2.6, the Zhujiang River basin under RCP8.5, and parts of the northwest river basins under all RCPs (Fig. 6d–f). About 50, 51, and 38% of all grids in the Songhuajiang, Liaohe, and Haihe
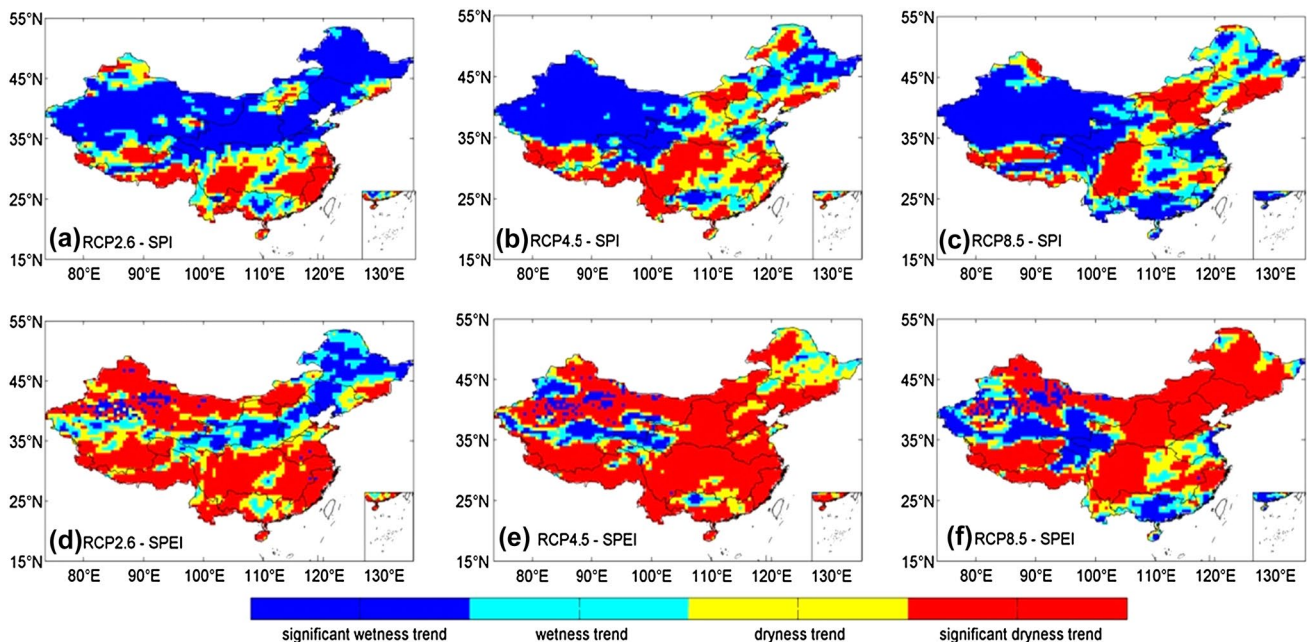

Fig. 6 Spatial distribution of projected changes in CCLM-simulated SPI (**a–c**) and SPEI (**d–f**) under RCP2.6, RCP4.5 and RCP8.5 over China for the period 2016–2050 relative to the period 1961–2005; The significance is based on the two-sample *t* test at 0.05 significance level

River basinsare projected with a significant wetness trend under RCP2.6, respectively. Similarly, around 42% of all grids in the Zhujiang River basin show significant trends towards wet conditions under RCP8.5.

3.3 Projected changes in drought frequency and duration

To identify the relative changes in drought frequency, the annual number of drought events is compared between the future period 2016–2050 and the baseline period 1961–2005 at each grid without considering the drought extent. By using the SPI, the regional variations in drought frequency under RCP2.6, RCP4.5, and RCP8.5 for the period 2016–2050 relative to the baseline period 1961–2005 are shown in Fig. 7a–c. Under RCP2.6, droughts occur more frequently in the Southwest and the Southeast river basins. The relative changes in drought frequency can be up to 264%. Under RCP4.5, the number of droughts is projected to increase in the Southwest river basins, the Yangtze River basin, the middle of the Yellow River basin, the Haihe River basin, and in parts of the Liaohe and Songhuajing River basins. Under RCP8.5, most frequent drought events occur in the observed southwest to northeast dryness band. For all RCPs, the projected changes in drought frequency to more occurrences are generally located in the southwest of China, while more drought events are mainly projected in the eastern, central,

and northeastern river basins with increasing emission concentration levels, respectively. The changes in SPEI-based drought frequency (Fig. 7d–f) in South China are similar to the SPI under all three RCPs, while different tendencies are mainly located in North China with most of the grids having an increasing tendency, especially in the northwest river basins.

The average drought duration is calculated by averaging the duration of all droughts simulated in the baseline period 1961–2005 and likewise the projected future period 2016–2050 at each grid. The relative changes in drought duration between these study periods are then compared and illustrated (Fig. 8). For the SPI-based analysis under RCP2.6, the projected drought duration will mainly increase in parts of the Southwest, Zhujiang, Yangtze, and Southeast river basins, while other regions show decreasing tendencies in drought duration. Under RCP4.5, regions with tendencies toward longer duration are additionally found in some parts of the northeastern river basins. Here, the maximum relative change is up to 215%. Under RCP8.5, even more regions with increasing drought durations are projected. These regions mainly include the river basins along the previously mentioned southwest to northeast dryness band. Under all RCPs, droughts especially in the southwest and southeast of China are projected with prolonged duration. For the SPEI-based analysis of drought duration, relative to 1961–2005, tendencies toward shorter duration are mainly found in the Zhujiang and the northeastern river
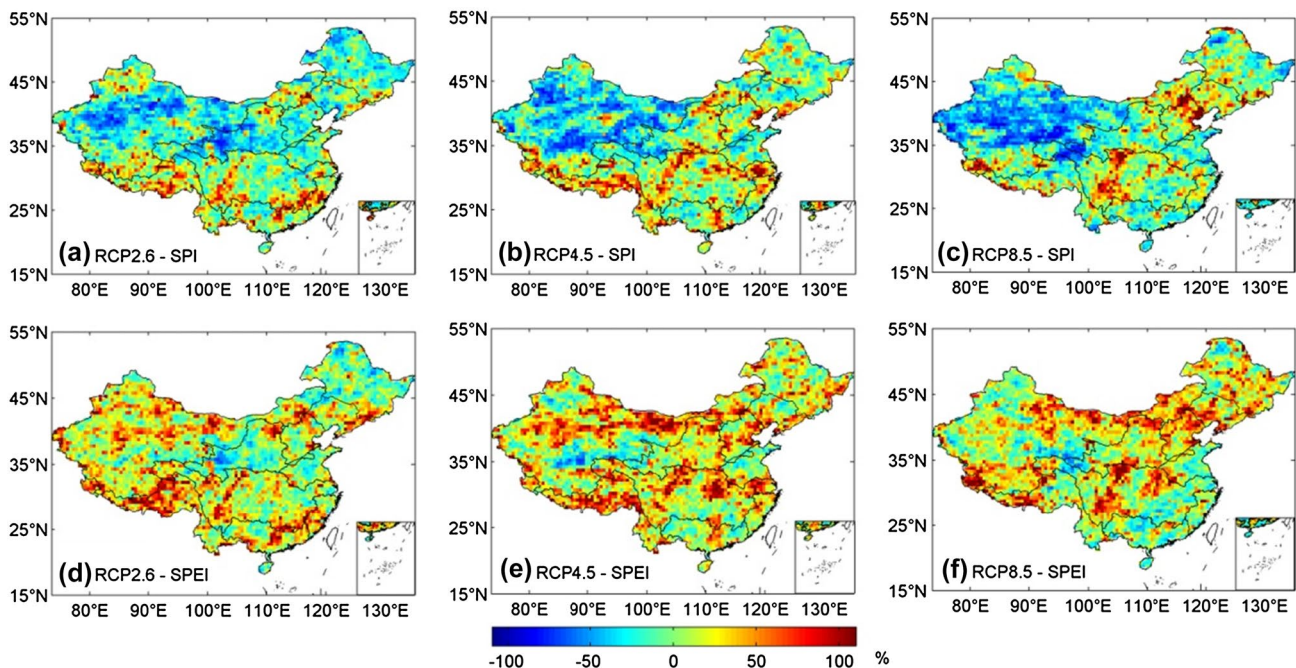

Fig. 7 Spatial distribution of projected changes in the CCLM-simulated drought frequency detected by SPI (**a–c**) and SPEI (**d–f**) under RCP2.6 (**a, d**), RCP4.5 (**b, e**), and RCP8.5 (**c, f**) over China during 2016–2050 relative to the period 1961–2005
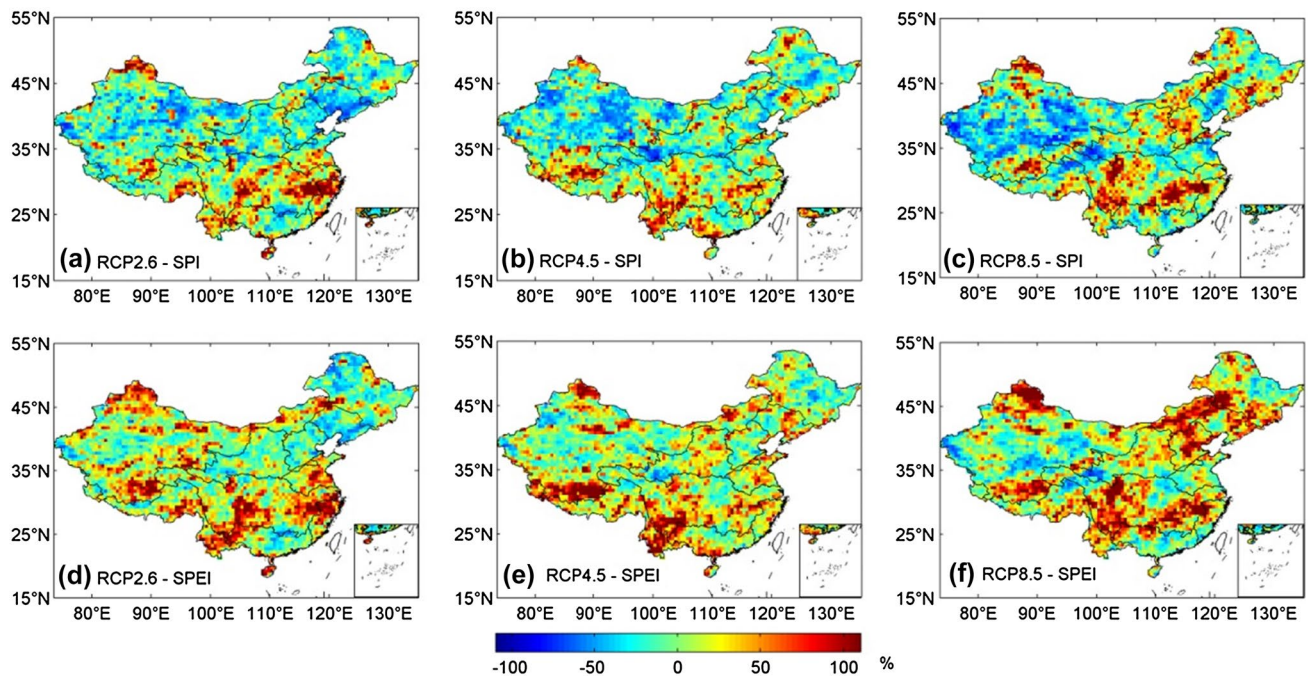
Fig. 8 Spatial distribution of projected changes in the CCLM-simulated drought duration detected by SPI (**a–c**) and SPEI (**d–f**) under RCP2.6 (**a, d**), RCP4.5 (**b, e**), and RCP8.5 (**c, f**) over China during 2016–2050 relative to the period 1961–2005

basins, while droughts with a longer duration are projected in the Yangtze, Southwest, and Southeast river basins under RCP2.6. Similar spatial patterns are also found under RCP4.5 and RCP8.5. From the low emission to high emission, droughts with longer duration are projected in the middle and lower Yangtze River basin.

3.4 Projected changes in drought area

At a space–time dimension, each drought event has a spatial extent. The average area of drought events with different duration identified by SPI or SPEI is calculated by averaging the area of all drought events. The number of drought events per year is counted by considering the spatial extent. Relative changes in drought area and number between the baseline period 1961–2005 and the future period 2016–2050 are shown in Fig. 9.

The SPI-based changes under RCP2.6 show areas of short-term drought events (1–3 months) with a slight decreasing tendency, while strong increases of up to 48% are found for long-term drought events (>12 months). All drought events with different duration have a decreasing tendency in area under RCP4.5, while increasing tendencies in drought area are projected under RCP8.5. Here, the increases in drought area with a 24-month duration are up to 60%. Relative to the baseline period, decreasing changes in frequency are found in short term (1–3 months) drought events, while increases are projected in medium- and

long-term drought events (>9 months) under both RCP2.6 and RCP8.5. Under RCP4.5, increasing changes are shown in drought events with duration of less than 12 months, while the frequency of long-term drought events (>12 months) decreases.

For SPEI-based changes (Fig. 9c, d), all RCPs show an increasing tendency in drought area for different duration. Large increases are found in short-term (1–3 months) and long-term (>12 months) drought events. The drought number also shows increasing tendencies under all RCPs. The relative changes in drought events with 24-month duration can reach 473, 594, and 1073% for RCP2.6, RCP4.5, and RCP8.5, respectively. Longer drought events are projected to be more frequent in future.

To identify the spatial changes in drought area, the location of the drought center per event (grid of the lowest SPI/ SPEI in the spatial extent) is extracted. Changes in the location of the drought center for different drought duration are shown in Fig. 10. As indicated by the SPI, drought events with 1-month duration will shift to the southwest under RCP2.6, while drought events with duration longer than 6 months are projected to move to the southeast. Under RCP4.5, drought events with different durations are projected to follow a southeastward shift. An eastward shift in drought centers is also found under RCP8.5. For the SPEI-based analysis, all durations follow a shift to the southwest under RCP2.6, except for the southeastward shift found in drought events with 24 months. Under RCP4.5, short- and
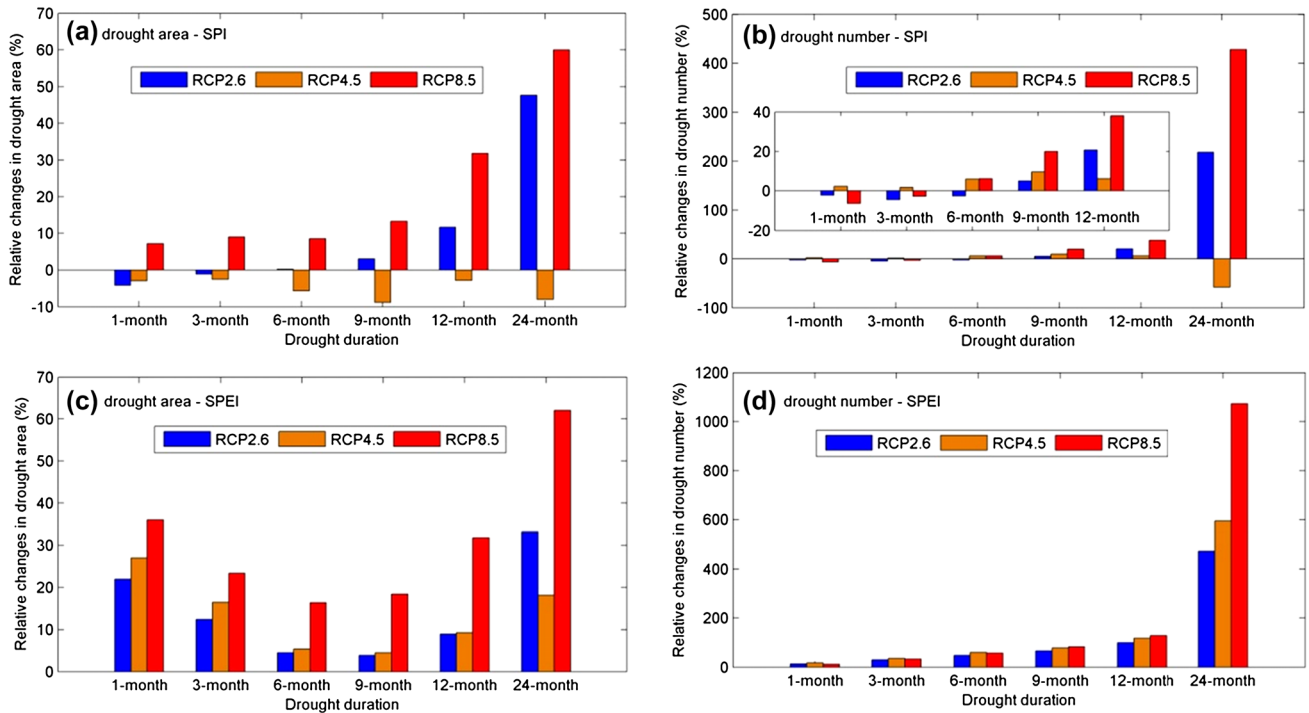
Fig. 9 Relative changes in drought area (**a, c**) and drought number (**b, d**) based on the SPI (**a–b**) and SPEI (**c–d**) for various durations and under three RCPs over China during the period of 2016–2050

Fig. 10 Shift of the drought center of drought events based on the SPI (*bold arrow*) and SPEI (*dashed arrow*) with a contiguous area larger than 50,000 km^2 for different durations and under three RCPs over China for the period 2016–2050 relative to the baseline period 1961–2005
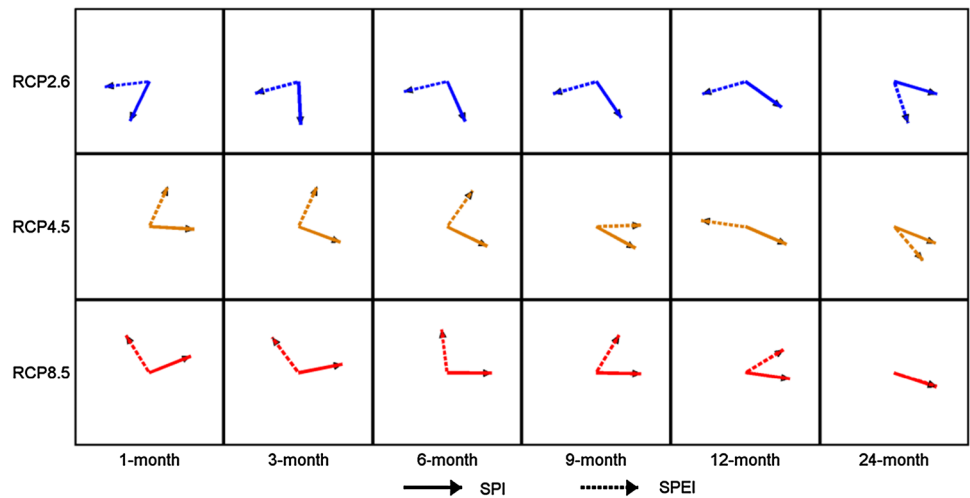
medium-term (1–6 months) drought events move to the northeast relative to the baseline period 1961–2005. A southeastward shift is also projected in drought events with 24 months duration. Under RCP8.5, northeast and northwest shifts of the location of drought events have been found for durations less than 12 months, while drought events with 24 months show a southeastward shift. Although different results are found between SPI and SPEI, consistent changes are shown in the location of the center of drought events with 24 months.

3.5 Severity of projected drought events

The IAD envelope curves represent the highest intensity at each contiguous drought area during the study period for whole China. A comparison of past and future envelope curves and projected single events is done to assess whether the drought events with predefined duration in future are more severe than the past drought events. In Fig. 11, the IAD envelope curve of the baseline period is
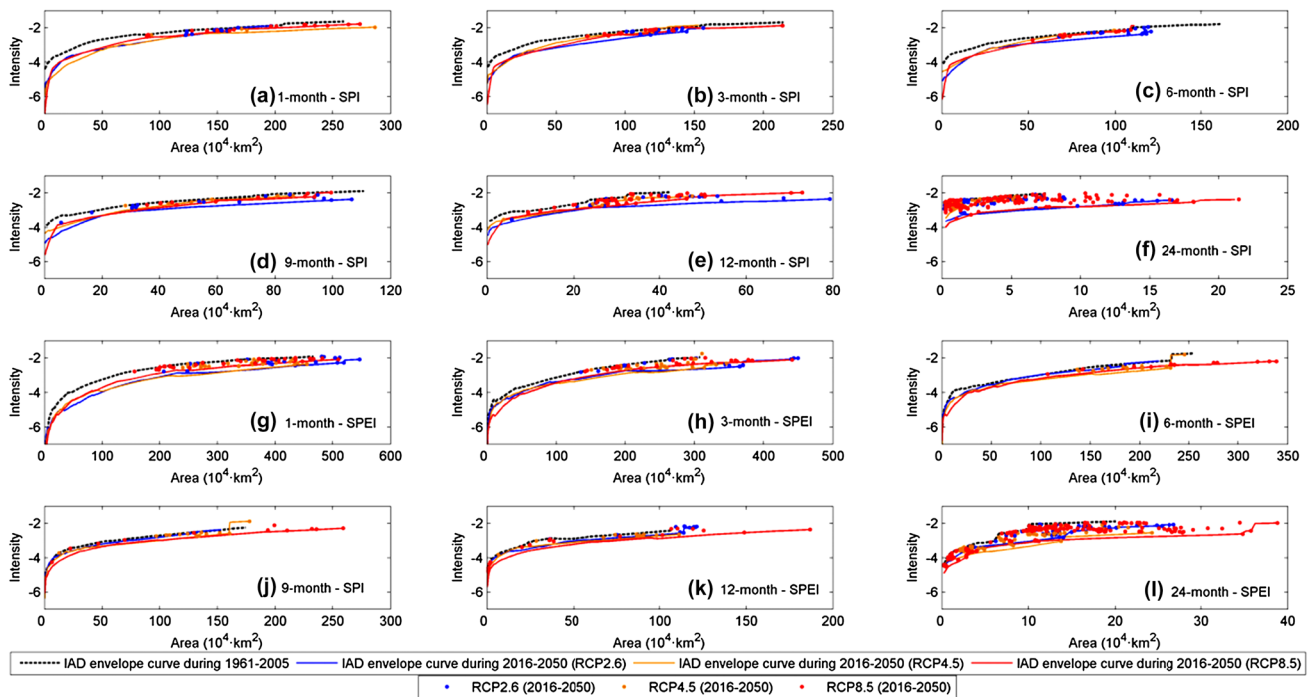
Fig. 11 Intensity-area-duration *envelope curves* and severe drought events (more severe than the baseline period) based on the SPI (**a–f**) and SPEI (**g–l**) under different RCPs over China for the period of 2016–2050 and the baseline period (1961–2005)

compared with the respective curves of the future period for each RCP.

The SPI-based analysis of IAD curves and severe drought events is presented in Fig. 11a–f. For droughts with 1-month duration, the envelope curves show quite similar paths (Fig. 11a), with the future curves having higher intensities under all RCPs. By considering both drought intensity and drought area under all RCPs, between four to seventeen future drought events of 1-month duration with an area above 50,000 km^2 are more severe than the most severe droughts of the baseline period (Table 2). For drought events with 3-months duration, from two to 16 drought events are projected to be more severe than in the past. Higher intensities are found for future IAD envelope curves at almost all contiguous areas. This is also found for drought events with 6- and 9-month duration (Fig. 11c–d).

The strongest change to higher intensities and high numbers of more severe drought events is projected for events with 12- and 24-months duration (Fig. 11f). In contrast to the baseline period, drought events with 12- and 24-months duration cover even larger areas under RCP2.6 and RCP8.5. Under RCP8.5, some 58 events are projected to be more severe than any 24-months-drought simulated in the past. Relative to the baseline period, the projected number of more severe drought events generally increases with increasing drought duration (Table 2).

The SPEI-based analysis of IAD curves and severe drought events is shown in Fig. 11g–l. Drought events with different durations cover even larger areas under RCP8.5 than in the baseline period. Short-term (1–3 months) and long-term (>12 months) drought events have a higher number of severe drought events than short-to-medium-term

Table 2 Number of CCLM-projected drought events in China (2016–2050), which are more severe than events in the baseline period (1961–2005); the projected droughts are categorized by their duration, all cover a contiguous area larger than 50,000 km^2, and they are based on the SPI or SPEI under three RCPs	Event duration (months)	SPI			SPEI		
		RCP2.6	RCP4.5	RCP8.5	RCP2.6	RCP4.5	RCP8.5
	1	11	4	17	22	26	33
	3	15	2	16	18	27	25
	6	15	3	9	2	14	12
	9	16	6	11	2	13	11
	12	24	9	43	12	11	13
	24	30	4	58	47	59	132

(4–6 months) and medium-term (7–12 months). The strongest change to higher intensities and high numbers of more severe drought events is also projected for events with 24-months duration. From low emission to high emission, higher numbers of drought events are projected. Under RCP8.5, the number of drought events more severe than in the baseline period with 24-months duration is 132 (Table 2). This means that for whole China long-lasting drought events of 24-months duration are very likely to be more severe (in intensity and/or areal extent) in the future.

The locations of the centers of severe drought events (more severe than events in the baseline period) for the period 2016–2050 are analyzed for all three RCPs (Fig. 12). For the SPI-based droughts under RCP2.6, the severe droughts show a southeastward shift in the 2020s and 2030s, and an eastward shift in the 2040s. Under RCP4.5, the projected locations of the centers of severe drought events are mainly located in the south of China, implying a southeastward shift compared to the baseline period. Under RCP8.5, many severe drought events also show a southeastward shift, while some others show shifts to the northeast or northwest. For the SPEI-based locations of the drought centers, a general southeastward shift is found under all RCPs. Some shifts to the east and to the northeast can also be detected under RCP8.5. By visualizing the location of the most severe drought centers, quite a large difference in the regional distribution of projected droughts based on the

SPI as compared to the SPEI can be seen. While the main concentration of SPI-based severe droughts is projected in South China, the SPEI-based severe droughts concentrate mostly in the northwest of China.

3.6 Projected changes in the wind field at 850 hPa

Projected changes in the summer and winter wind fields at 850 hPa during the period of 2016–2050 are shown in Fig. 13. Relative to 1961–2005, the rare changes in wind direction are less than 45 degrees, indicating only little changes in wind direction for both summer and winter during 2016–2050 under the three RCPs. In summer (June–August, JJA), similar changes in spatial patterns of wind speed are found under all RCPs. Increasing tendencies are shown in the Bay of Bengal, the South China Sea, the western Pacific and west of Eurasia, while decreases are projected in South of China. Differences are found in Northeast China with decreasing tendencies under RCP2.6 and increasing tendencies under RCP4.5 and RCP8.5. From low to high emission pathways, the wind speed gets stronger in the area of increases and weaker in the regions of decreasing tendencies (Fig. 13a–c). During the winter period (December–February, DJF), wet air flows come mainly from the west. Differences in wind speed changes under the three RCPs are mainly found for Northeast China and the North China Plain (Huaihe River basin, Haihe
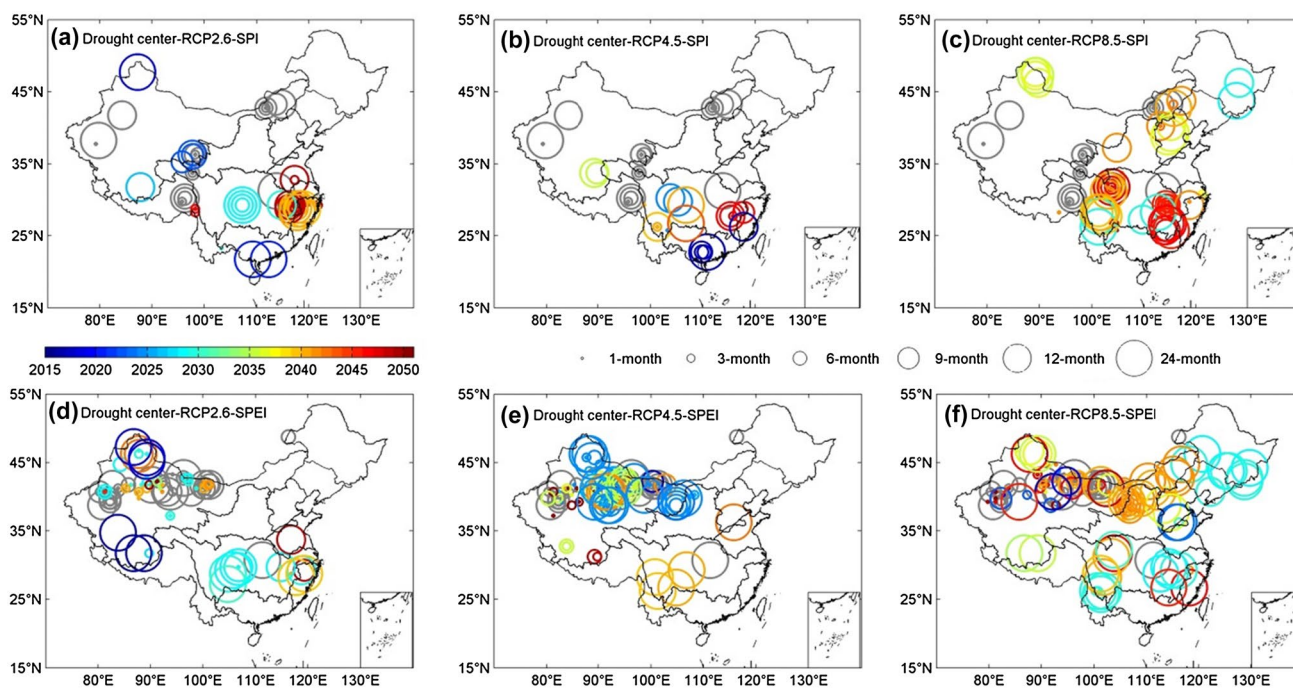

Fig. 12 Locations of severe drought events of specific duration (*circle* size) based on the SPI (**a–c**) and SPEI (**d–f**) under three RCPs in China for the baseline period (1961–2005, *grey circles*) and for the future period (2016–2050, *colored circles*); the colors denote the occurrence year of the drought events (more severe than during the baseline period)
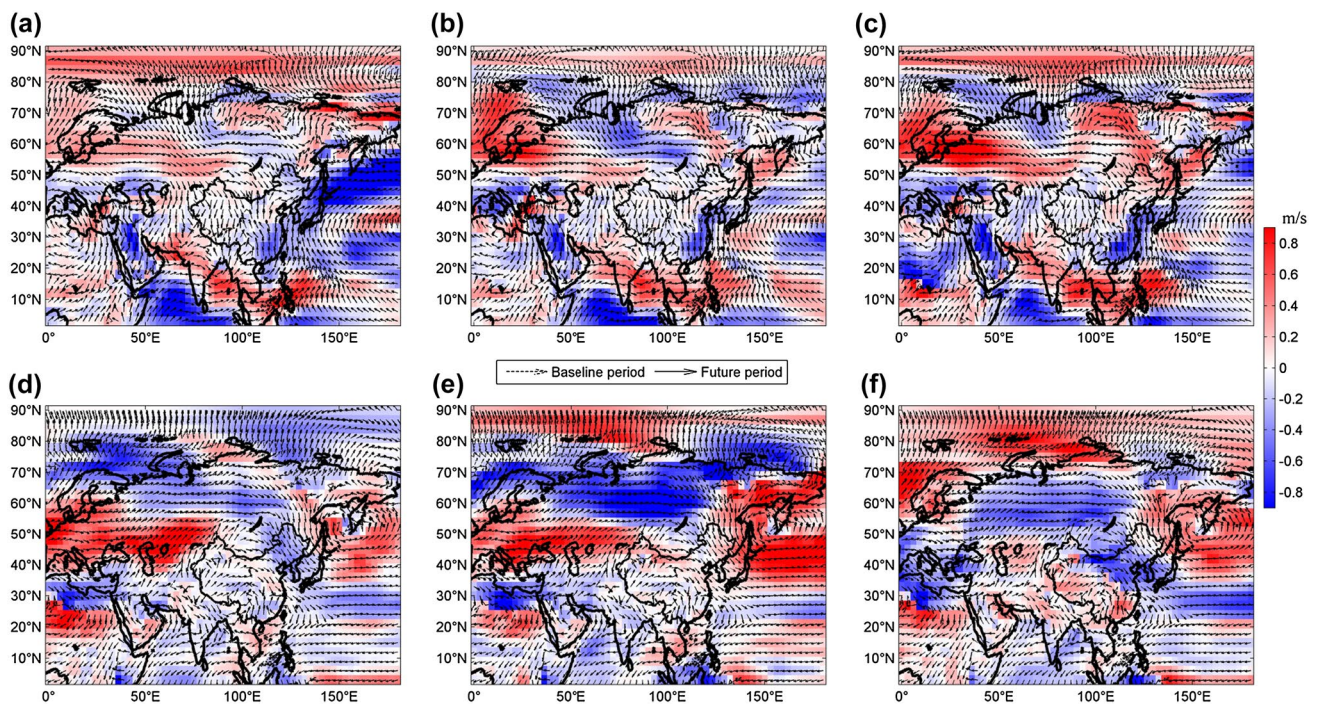
Fig. 13 Projected changes in the wind field at 850 hPa for summer (**a–c**) and winter (**d–f**) of 2016–2050 under RCP2.6 (**a, d**), RCP4.5 (**b, e**) and RCP8.5 (**c, f**) relative to 1961–2005; *arrows* represent the wind direction for the baseline period (*dotted*) and the future period (*solid*), while the *color shading* represents the difference in wind speed between the baseline and the future period

River basin and east of Yellow River basin). Decreasing tendencies are shown in Northeast China under RCP2.6, while increases are projected under both RCP4.5 and RCP8.5. Contrasting in the North China Plain, increasing tendencies are found under both RCP2.6 and RCP4.5, while decreases are projected under RCP8.5 (Fig. 13d–f).

4 Conclusions and discussion

The ability of CCLM in reproducing drought characteristics in China is evaluated on observed monthly climate datasets. Based on this, CCLM-projected changes in the intensity, area, and duration of future drought events are analyzed by applying the IAD method on SPI and SPEI time series for the period 2016–2050. Future analysis of drought characteristics is rather based on the SPEI-results, while the SPI is used in comparison with the SPEI to identify the effects of evapotranspiration on drought events.

Compared to the observations, the regional climate model CCLM has a certain capability to simulate the current climate (e.g. precipitation, evaporation) and drought characteristics in China. Dominant spatial features in annual precipitation are well reproduced by CCLM with significant SCCs around 0.71. But the variation in precipitation is hard to capture, the temporal correlation coefficient (TCC) between observation and simulations provided

by CMIP5 models over China is not significant or even negative (Xu and Xu 2012a). The simulation ability can be influenced by the biases in the driving GCM (Laprise 2014; Fischer et al. 2013). The MPI-ESM-LR, which is used to drive CCLM in this paper, shows a higher spatial and temporal correlation coefficient when compared to other CMIP5 GCMs (Xu and Xu 2012a).

The dominant spatial features in drought characteristics based on the SPI or SPEI are also well reproduced by CCLM, while significant higher numbers in drought events with shorter duration are simulated for the SPEI in the northwest of China. This may be related to the simulation ability in potential evapotranspiration. By using the Thornthwaite (TH) approach as described by Yu et al. (2014a, b), potential evapotranspiration can be well simulated, as temperature over China is satisfyingly captured by RCMs and even GCMs with spatial and temporal correlation coefficients above 0.90 (Gao et al. 2012b; Xu and Xu 2012a). Except contrasting tendencies between SPI- and SPEI-based drought events in the Northwest river basins, the Thornthwaite approach and the Penman–Monteith (PM) equation show similar results (Chen and Sun 2015). It has been found that the PM equation is more robust and can be computed with the climate variables provided by CCLM (Begueria et al. 2014). In addition, the dominant spatial features in observed potential evapotranspiration calculated with the PM equation could also be captured

with CCLM, especially for the northeastern river basins with SCCs above 0.80. The biases in PET from observations and simulation might be caused by the higher biases in relative humidity and sunshine duration, as well as the general assumptions of plant characteristics, which are very sensitive variables in the PET calculation for all regions of China (Yin et al. 2010).

Relative to the baseline period 1961–2005, in most of the future years (2016–2050) dry conditions according to the SPEI are projected for the ten large river basins. By comparing the results from the SPI and SPEI, it becomes clear that the northern river basins, including the Songhuajiang, Liaohe, Haihe, Yellow River, and the Northwest river basins, are heavily affected by evapotranspiration. In the Northwest river basins opposite drought conditions are found between the SPEI and SPI. However, the Yangtze, Zhujiang, Southwest, and Southeast river basins are less affected by evapotranspiration showing only small differences between the two drought indices. The responses of temperature and precipitation to drought in northern China are also larger for the baseline period (Chen and Sun 2015). This can also be seen in the spatial patterns of the changes in the CCLM-simulated SPI and SPEI, especially under the higher emission RCPs.

A dryness band from the southwest to the northeast of China has been observed for the period 1960–2013 (Zhai et al. 2016). A continuing tendency to dry conditions along this observed dryness band in China is projected under RCP4.5 and RCP8.5. Under RCP2.6, continuing dryness tendencies are found in Southwest China. Additional areas with tendencies to dryness under all RCPs are also found in the Southeast river basins, the middle and lower Yangtze River basin, and the Northwest river basins. These changes may lead to more serious drought events in Southwest China and an overall shift of drought events to the south. According to the differences between the spatial patterns of the SPI and SPEI, from low emission to high emission RCPs, the drought centers are more likely to experience a southeastward and northwestward shift mainly caused by the decrease in precipitation or the increase in evapotranspiration, respectively. The decrease in precipitation in the southern parts of China has also been projected with the CMIP5 multi-model ensemble, especially under RCP8.5 (Xu and Xu 2012b).

Based on the SPEI results, more frequent drought events with a longer duration will occur mainly in the Southwest and the middle and lower Yangtze River basins under RCP2.6 and RCP4.5 relative to the baseline period, which are the results of a projected reduction in precipitation amounts. Under RCP8.5, drought events with longer duration are more frequent in the southwest and northeast of China and less frequent in the southeast of China. Comparing the SPEI and SPI-results, evapotranspiration

plays an important role in the increase in drought number and duration in parts of the northern river basins. The similar changes under all RCPs are the higher drought numbers and longer duration in the southwest of China and the longer duration in the southeast. Comparable findings are also projected by other GCMs and RCMs, which use a similar drought index or the extreme climate index of consecutive dry days (CDD). By calculating the SPI drought index under a SRES A1B scenario (equivalent to RCP6.0), fewer droughts in northern China and more droughts in parts of southern China have also been projected (Chen et al. 2013). The projected CDD show an increase in the south of China, with the strongest increase found in the southwest, indicating an aggravation of drought risks, especially in southwestern China (Xu et al. 2013; Ji and Kang 2015). Furthermore, the drought risks, projected by the CMIP5 multi-model ensemble, show two major risk locations, one in the southwest of China and one in the Qinghai-Tibetan Plateau (Wang and Chen 2014).

The drought area is traditionally obtained either by considering its largest extent or by counting the affected (administrative) regions of China. The IAD method provides a good opportunity to analyze drought events in a space–time dimension by considering their spatial extent (in this study larger than 50,000 km^2) for different drought durations. Based on this, all drought events show increasing tendencies in drought area and number, especially for the long-term (>12 months) drought events. For the drought events detected by SPI only considering the decrease in precipitation, under RCP4.5 (the closest RCP to SRES A1B), the drought areas for all drought durations show decreasing tendencies, which is in line with the results described by Chen et al. (2013) who used SRES A1B. More severe drought events of small areal extent and duration less than 12 months are projected under RCP4.5 relative to the baseline period. Observed changes in China during 1960–2013 show a decreasing tendency in drought area but an increase in severity (Zhai et al. 2016). This tendency is projected to continue under RCP4.5. However, a higher frequency with increasing area extent is projected for drought events with more than 6 months duration under RCP2.6 and RCP8.5. According to the differences between the SPI and SPEI, global warming will lead to an increase in droughts with larger area and different duration. It should be noted that the actual projected monthly data is used in the identification of the future number of drought events under the different RCPs, hence taking the projections as some kind of real forecast instead of focusing on the underlying trends, for which the climate projections are implied for. That means the projected number in severe drought events inhibit a high uncertainty, which should be considered when comparing past and future drought events.

Without considering the effects of global warming, the locations of drought events with different durations are estimated to likely shift from the southwest to the east or southeast of China. The shift of the location of drought centers from the northwest to the southeast within Central China has also been found in observed time series (Zhai et al. 2016). By considering the evapotranspiration through assessing the SPEI, a relative northward shift of drought centers can be projected. However, the long-term (>12 months) drought events indicated by the SPI and SPEI are projected to shift to the southeast of China. To further quantify the intensity of future droughts, more severe drought events than experienced in the past can be extracted by the IAD method. From low emission to high emission RCPs, higher numbers of drought events more severe than in the past are projected, especially for the drought events with 24-months duration. Relative to most severe droughts in baseline period, the severe drought events in future are also expected to mainly shift southeastward.

Changes in droughts characteristics (and location shifts) are affected by the observed and projected decrease in precipitation and increase in evapotranspiration. Constant increases in evapotranspiration are projected for all regions of China, which is associated with global warming. The changes in precipitation are related to the changes in water vapor inflows. Differences in regional precipitation changes projected with three RCPs are mainly found in Northeast China and the North China Plain (Huaihe River basin, Haihe River basin and east of Yellow River basin). The decreasing tendencies in 850 hPa wind speed in Northeast China under RCP2.6 will lead to more precipitation than under RCP4.5 and RCP8.5. These changes result in a tendency to wetness in the northeast river basins of China under RCP2.6.

Conclusively, more frequent long-term drought events (>12 months) with large areas are more likely to occur in the south of China. This finding should be of great concern, as most droughts have rather adverse impacts in the socio-economic sectors of China, especially in the south of China (Qin et al. 2015). For example, the reduction in hydroelectrical production went up to 20% and significant impacts on the vegetation productivity had been detected in southwestern China during the 2009/2010 drought event (Barriopedro et al. 2012; Zhang et al. 2012). Shifts and increases in the intensity, area, and duration of future droughts will put more stress on the population, the agriculture, and the water resources in China. Therefore, adaptation measures at regional and local scale need to be implemented to be prepared for severe future drought impacts in China. Further research on local impacts of droughts and potential adaptation measures is of great demand. In addition, Multi RCM-ensembles under the CORDEX frame should be analyzed in further studies to address the uncertainties involved in regional climate projections (Giorgi et al. 2009; Giorgi and Gutowski 2015).

References

Allen RG, Pereira LS, Raes D, Smith M (1998) Crop evapotranspiration—guidelines for computing crop water requirements—FAO irrigation and drainage paper 56. FAO, Rome

Andreadis KM, Clark EA, Wood AW, Hamlet AF, Lettenmaier DP (2005) Twentieth-century drought in the conterminous United States. J Hydrometeorol 6:985–1001

Barriopedro D, Gouveia CM, Trigo RM, Wang L (2012) The 2009/10 drought in China: Possible causes and impacts on vegetation. J Hydrometeorol 13:1251–1267

Begueria S, Vicente-Serrano SM, Reig F, Latorre B (2014) Standardized precipitation evapotranspiration index (SPEI) revisited: parameter fitting, evapotranspiration models, tools, datasets and drought monitoring. Int J Climatol 34(10):3001–3023

Biondi F, Kozubowski TJ, Panorska AK, Saito L (2008) A new stochastic model of episode peak and duration for eco-hydro-climatic applications. Ecol Modell 211(3–4):383–395

Bordi I, Sutera A (2002) An analysis in Italy in the last 50 years. IL Nuovo Cimento, 25C:185–206

Burke EJ, Brown SJ (2007) Evaluating uncertainties in the projection of future drought. J Hydrometeorol 9:292–299

Cai W, Purich A, Cowan T, van Rensch P, Weller E (2014) Did climate change-induced rainfall trends contribute to the Australian millennium drought? J Climate 27:3145–3168

Cao LG, Zhong J, Su BD, Zhai JQ, Macro G (2013) Probability distribution and projected trends of daily precipitation in China. Adv Clim Change Res 4(3):153–159

Chen HP, Sun JQ (2015) Changes in drought characteristics over China using the Standardized precipitation evapotranspiration index. J Clim 28:5430–5447

Chen HP, Sun JQ, Chen XL. 2013. Future changes of drought and flood events in China under a global warming scenario. Atmos Ocean Sci Lett 6(1):8–13

Collins M, Knutti R, Arblaster JM, Dufresne JL, Fichefet T, Friedlingstein P, Gao X, Gutowski WJ, Johns T, Krinner G, Shongwe M, Tebaldi C, Weaver AJ, Wehner M (2013) Long-term climate change: projections, comments and irreversibility. In: Climate Change 2013: the physical science basis. Contribution of working group I to the Fifth Assessment Report of the Intergovernmental Panel on Climate Change. Stocker TF, Qin D, Plattner GK et al. Cambridge University Press, Cambridge, pp 1029–1136

Dai A (2013) Increasing drought under global warming in observations and models. Nature. Clim Change 3:52–58

Duffy PB, Brando P, Asner GP, Field CB (2015) Projections of future meteorological drought and wet periods in the Amazon. Proc Natl Acad Sci 112(43):13172–13177

Field CB, Barros V, Stocker TF, Qin D, Dokken DJ, Ebi KL, Mastrandrea MD, Mach KJ, Plattner GK, Allen SK, Tignor M, Midgley PM, IPCC (2012) Managing the risks of extreme events and disasters to advance climate change adaptation. Cambridge University Press, Cambridge, pp 582

Fischer T, Gemmer M, Liu L, Su BD (2011) Temperature and precipitation trends and dryness/wetness pattern in the Zhujiang River Basin, South China, 1961–2007. Quat Int 244(2):138–148

Fischer T, Menz C, Su BD, Scholten T (2013) Simulated and projected climate extremes in the Zhujiang River Basin, South China, using the regional climate model COSMO-CLM. J Climatol 33:2988–3001

Gao X, Xu Y, Zhao Z, Pal JS, Giorgi F (2006) On the role of resolution and topography in the simulation of East Asia precipitation. Theor Appl Climatol 86(1):173–185

Gao X, Shi Y, Zhang D, Wu J, Giorgi F, Ji Z, Wang Y (2012a) Uncertainties in monsoon precipitation projections over China: results from two high-resolution RCM simulations. Clim Res 52:213–226.

Gao X, Shi Y, Zhang DF, Giorgi F (2012b) Climate change in China in the 21st century as simulated by a high resolution regional climate model. Chin Sci Bull 57(10):1188–1195

Gemmer M, Jiang T, Su BD, Kundzewicz ZW (2008) Seasonal precipitation changes in the wet season and their influence on flood/drought hazards in the Yangtze River Basin, China. Quat Int 186:12–21

Giorgetta M, Jungclaus J, Reick C, Legutke S, Bader J, Böttinger M, Brovkin V, Crueger T, Esch M, Fieg K, Glushak K, Gayler V, Haak H, Hollweg H-D, Ilyina T, Kinne S, Kornblueh L, Matei D, Mauritsen T, Mikolajewicz U, Mueller W, Notz D, Pithan F, Raddatz T, Rast S, Redler R, Roeckner E, Schmidt H, Schnur R, Segschneider J, Six K, Stockhause M, Timmreck C, Wegner J, Widmann H, Wieners K-H, Claussen M, Marotzke J, Stevens B (2013) Climate and carbon cycle changes from 1850 to 2100 in MPI-ESM simulations for the coupled model intercomparison project phase 5. J Adv Model Earth Syst 5:572–597. doi:10.1002/jame.20038.

Giorgi F, Gutowski Jr W (2015) Regional dynamical downscaling and the CORDEX initiative. Annu Rev Environ Resour 40:467–490

Giorgi F, Colin J, Ghassem RA (2009) Addressing climate information needs at the regional level: the CORDEX framework. WMO Bull 58(3):175–183

Hansen J, Ruedy R, Sato M et al (2010) Global surface temperature change. Rev Geophys 48:Rg4004

Hirabayashi Y, Kanae S, Emori S, Oki T, Kimoto M (2008) Global projections of changing risk of floods and droughts in a changing climate. J Geophys Res 53(4):754–772

Ji Z, Kang S (2015) Evaluation of extreme climate events using a regional climate model for China. Int J Climatol 35:888–902

Kim DW, Byun HR (2009) Future pattern of Asian drought under global warming. Theor Appl Climatol 98:137–150

Laprise R (2014) Comment on "The added value to global model projections of climate change by dynamical downscaling: a case study over the continental U.S. using the GISS-ModelE2 and WRF models" by Racherla et al. J Geophys Res Atmos 119:3877–3881

Liang XZ, Li L, Kunkel KE (2004) Regional climate model simulation of U.S. precipitation during 1982–2002. Part I: annual cycle. J Clim 17:3510–3529

Liang XZ, Kunkel KE, Meehl GA, Jones RG, Wang JXL (2008) Regional climate models downscaling analysis of general circulation models present climate biases propagation into future change projections. Geophys Res Lett 35:L08709. doi:10.1029/2007GL032849

Liu K, Jiang DB, Ma JY (2012) Drought over China in the 21st century: results of RegCM3. Atmos Ocean Sci Lett 5(6):509–513.

McKee TB, Doesken NJ, Kleist J (1993) The relationship of drought frequency and duration to time scales. Preprints, Eighth Conf. on Applied Climatology, Anaheim, CA, Am Meteor Soc, pp 179–184

McMahon TA, Peel MC, Karoly DJ (2015) Assessment of precipitation and temperature data from CMIP3 global climate models for hydrologic simulation. Hydrol Earth Syst Sci 19:361–377

Meehl GA, Boer GJ, Covey C, Latif M, stouffer RJ (2000) The coupled model intercomparison project (CMIP). Bull Am Meteorol Soc 81:313–318

Meehl GA, Stocker TF, Collins WD et al. 2007. Global climate projection. In: Climate change 2007: the physical science basis. Contribution of working group I to the fourth assessment report of the Intergovernmental Panel on Climate Change. Cambridge University Press, 747–845

Nasrollahi N, AghaKouchak A, Cheng L, Damberg L, Phillips TJ, Miao C, Hsu K, Soroosshian S (2014) How well do CMIP5 climate simulations replicate historical trends and patterns of meteorological droughts? Water Resour Res 51(4):2847–2864

Orlowsky B, Seneviratne SI (2013) Elusive drought: uncertainty in observed trends and short- and long-term CMIP5 projections. Hydrol Earth Syst Sci 17:1765–1781

PaiMazumder D, Done JM (2014) Uncertainties in long-term drought characteristics over the Canadian Prairie provinces, as simulated by the Canadian RCM. Clim Res 58 209–220. doi:10.3354/cr01196

Park CK, Byun HR, Deo R, Lee BR (2015) Drought prediction till 2100 under RCP 8.5 climate change scenarios for Korea. J Hydrol 526:221–230

Qian WH, Shan XH, Zhu YF (2011) Ranking regional drought events in China for 1960–2009. Adv Atmos Sci 28(2):310–321

Qin DH, Zhang JY, Shan CC et al (2015) China national assessment report on risk management and adaptation of climate extremes and disasters. Science Press, Beijing, pp 70–124

Raisanen J (2007) How reliable are climate models? Tellus A 59:2–29

Reifen C, Toumi R (2009) Climate projections: past performance on guarantee of future skill? Geophys Res Lett 36:L13704

Rockel B, Will A, Hense A (2008) The regional climate model COSMO-CLM(CCLM). Meteorol Z 17(4):347–348

Rohde R, Muller RA, Jacobsen R et al (2013) A new estimate of average earth surface land temperature spanning 1753 to 2011. Geoinfor Geostat Overv 1(1):1–7

Seneviratne SI (2012) Historical drought trends revisited. Nature 495:338–339

Sheffield J, Wood EF (2007) Characteristics of global and regional drought, 1950–2000: Analysis of soil moisture data from off-line simulation of the terrestrial hydrologic cycle. J Geophys Res 112:D17115

Sheffield J, Wood EF (2008) Projected changes in drought occurrence under future global warming from multi-model, multi-scenario, IPCC AR4 simulations. Clim Dyn 31:79–105

Sheffield J, Andreadis KM, Wood EF, Lettenmaier DP (2009) Global and continental drought in the second half of the twentieth century: severity-area-duration analysis and temporal variability of large-scale events. J Clim 22(8):1962–1981

Shi YF, Shen YP, Li DL et al (2003) Discussion on the present climate change from warm-dry to warm-wet in Northwest China. Quat Sci 23:152–164

Sun C, Yang S (2012) Persistent severe drought in southern China during winter-spring 2011: large-scale circulation patterns and possible impacts factors. J Geophys Res 117:D10112

Svoboda MD, Fuchs BA, Poulsen CC, Nothwehr JR (2015) The drought risk atlas: Enhancing decision support for drought risk management in the United States. J Hydrol 523:274–286

Tao H, Borth H, Fraedrich K, Su BD, Zhu XH (2014) Drought and wetness variability in the Tarim River Basin and

connection to large-scale atmospheric circulation. Int J Climatol 34(8):2678–2684

Taylor KE, Stouffer RJ, Meehl GA (2012) An overview of CMIP5 and the experiment design. Bull Am Meteor Soc 934:485–498. doi:10.1175/BAMS-D-11-00094.1

Van Vuuren DP, Edmonds J, Kainuma M, Riahi K, Thomson A, Hibbard K, Hurtt GC, Kram T, Krey V, Lamarque JF, Masui T, Meinshausen M, Nakicenovic N, Smith SJ, Rose SK (2011) The representative concentration pathways: an overview. Clim Change. doi:10.1007/s10584-011-0148-z

Vicente-Serrano SM, Begueria S, Lopez-Moreno JI (2010) A multiscalar drought index sensitive to global warming: the standardized precipitation evapotranspiration index. J Clim 23:1696–1718

Vicente-Serrano S M, Begueria S, Lorenzo-Lacruz J, Camarero JJ, Lopez-Moreno JI, Azorin-Molina C, Revuelto J, Moran-Tejeda E, Sanchez-Lorenzo A (2012) Performance of drought indices for ecological, agricultural, and hydrological applications. Earth Interact 16(10):1–27

Wang G (2005) Agricultural drought in a future climate: results from 15 global climate models participating in the IPCC 4th assessment. Clim Dyn 25(7–8):739–753

Wang L, Chen W (2014) A CMIP5 multimodel projection of future temperature, precipitation, and climatological drought in China. Int J Climatol 34:2059–2078

Wang D, Menz C, Simon T, Simmer C, Ohlwein C (2013) Regional dynamical downscaling with CCLM over East Asia. Meteorol Atmos Phys 121:39–53

Wehner M, Easterling DR, Lawrimore JH et al (2011) Projections of future drought in the continental UnitedStates and Mexico. J Hydrometeorol 12:1359–1376

Wong G, Van Lanen HAJ, Torfs P (2013) Probabilistic analysis of hydrological drought characteristics using meteorological drought. Hydrol Sci J 58(2):253–270

World Meteorological Organization (WMO) (2012) Standardized precipitation index user guide (WMO-No.1090), Geneva

Wu H, Hayes MJ, Wilhite DA et al (2005) The effect of the length of record on the standardized precipitation index calculation. Int J Climatol 25:505–520

Xu Y, Xu CH. 2012a. Preliminary assessment of simulations of climate changes over China by CMIP5 Multi-models. Atmos Ocean Sci Lett 5(6):489–494

Xu CH, Xu Y. (2012b) The projection of temperature and preipitation over China under RCP scenarios using a CMIP5 multi-model ensemble. Atmos Ocean Sci Lett 5(6):527–533.

Xu JY, Shi Y, Gao XJ, Giorgi F (2013) Projected changes in climate extremes over China in the 21st century from a high resolution regional climate model (RegCM3). Chin Sci Bull 58:1443–1452

Xu K, Yang DW, Yang HB, Li Z, Qin Y, Shen Y (2015) Spatio-temporal variation of drought in China during 1961–2012: a climatic perspective. J Hydrol 526:253–264

Yang CG, Yu ZB, Hao ZC, Zhang JY, Zhu JT (2012) Impact of climate change on flood and drought events in Huaihe River Basin, China. Hydrol Res 43(1–2):14–22

Yin Y, Wu S, Chen G, Dai E (2010) Attribution analyses of potential evapotranspiration changes in China since the 1960s. Theor Appl Climatol 101:19–28

Yin Y, Ma D, Wu S, Pan T (2015) Projections of aridity and its regional variability over China in the mid-21st century. Int J Climatol 35(14):4387–4398. doi:10.1002/joc.4295

Yu ET, Wang HJ, Sun JQ (2010) A quick report on a dynamical downscaling sumulation over China using the nested model. Atmos Ocean Sci Lett 3(6):325–329

Yu X, He X, Zheng H, Guo R, Ren Z, Zhang D, Lin J (2014a) Spatial and temporal analysis of drought risk during the crop-growing season over northeast China. Nat Hazards 71(1):275–289

Yu MX, Li QF, Hayes MJ, Svoboda MD, Heim RR (2014b) Are droughts becoming more frequent or severe in China based on the standardized precipitation evapotranspiration index: 1951–2010? Int J Climatol 34:545–558

Zarch MAA, Sivakumar B, Sharma A (2015) Droughts in a warming cliamte: A global assessment of Standardized precipitation index (SPI) and Reconnaissance drought index (RDI). J Hydrol 526:183–195

Zhai JQ, Su BD, Krysanova V, Gao C, Jiang T (2010a) Spatial variation and trends in PDSI and SPI indices and their relation to streamflow in 10 large regions of China. J Clim 23:649–663

Zhai JQ, Liu B, Hartmann H, Su BD, Jiang T, Fraedrich K (2010b) Dryness/wetness variations in ten large river basins of China during the first 50 years of the 21st century. Quat Int 226:101–111

Zhai JQ, Gao B, Zhu XY (2014) Fact sheet on climate disasters in China. In: Wang G W, Zheng GG (eds) Annual report on actions to address climate change. Social Sciences Academic Press, Beijing

Zhai JQ, Huang JL, Su BD, Cao LG, Wang YJ, Jiang T, Fischer T (2016) Intensity-area-duration analysis on droughts in China. Clim Dyn. doi:10.1007/s00382-016-3066-y

Zhang L, Xiao J, Li J, Wang K, Lei L, Guo H (2012) The 2010 spring drought reduced primary productivity in southwestern China. Environ Res Lett 7. doi:10.1088/1748-9326/7/4/045706

Zhang MJ, He JY, Wang BL, Wang SJ, Li SS, Liu WL, Ma XN (2013) Extreme drought changes in Southwest China from 1960 to 2009. J Geog Sci 23(1):3–16

Zhao GJ, Mu XM, Hörmann G, Fohrer N, Xiong M, Su BD, Li XC (2012) Spatial patterns and temporal variability of dryness/wetness in the Yangtze River Basin, China. Quat Int 282:5–13